Laser-induced periodic surface structure. II. Experiments on Ge, Si, Al, and brass

Jeff F. Young, J. S. Preston, H. M. van Driel, and J. E. Sipe
Department of Physics and Erindale College, University of Toronto, Toronto, Ontario M5S 1A7, Canada
(Received 20 April 1982)

We report the results of a detailed investigation into the properties of the periodic damage structure that can be produced on nominally smooth surfaces of solids when they are irradiated with a single beam of intense laser radiation. The study is primarily concerned with extracting information from the Fourier transform of the damage structure as observed via the Fraunhofer diffraction pattern produced by reflecting a cw laser beam from the surface. In particular, the patterns produced in Ge, Si, Al, and brass by pulsed 1.06- and 0.53-μm radiation are compared as a function of the angle of incidence and polarization of the beam. We find that all materials contain similar and much more intricate detailed structure than has been previously appreciated. Whereas periodic ripple patterns oriented perpendicular to the polarization at near-normal incidence are commonly reported, the diffraction patterns reveal that in fact there exists a continuous distribution of periodic structure oriented at all angles with respect to the polarization. At near-normal incidence there are two dominant sets of "fringes" running perpendicular to the polarization, while for a *p*-polarized beam incident at $>35°$ there exist three dominant periodic structures; two which run perpendicular to the polarization and one which is oriented parallel to it. For *s*-polarized light incident at angles $>35°$ there are two dominant patterns which form a cross-hatched pattern with axes oriented at 45° to the plane of incidence. A study of the evolution of the patterns on a shot-to-shot basis indicates that both the initial and laser-induced surface roughness play important roles in the evolution of the damage. We conclude with a comparison of our experimental results with those predicted by the theory developed in the preceding paper. Excellent agreement is found.

I. INTRODUCTION

Laser-induced damage of solids has been an area of both theoretical and experimental interest ever since the development of the laser itself.[1] Advances in this field are certainly important to pure research on the interaction of high-intensity optical pulses with matter, and are of prime interest in applied physics to the achievement of maximum transmissivity and reflectivity of optical components for high-intensity laser beams. In addition, pulsed-laser semiconductor annealing[2] and device fabrication[3] have become important examples of how controlled laser "damage" can be used to alter the optical or electrical properties of materials in a beneficial manner. In some areas of damage research progress has occurred only on an empirical basis because of different material properties or the presence of various kinds of defects. The irregularity of the bulk or surface damage structure and the sharp threshold associated with damage has, in many cases, prevented a complete characterization of the damage process in terms of intrinsic or extrinsic (defect) material properties.

Over the past seventeen years, however, one form of laser surface damage which appears to be spatially periodic in nature, and which occurs on a wide variety of both opaque and transparent materials, has been noted by several authors. Birnbaum[4] first reported this gratinglike damage that occurred on the surface of various semiconductor materials which were used as *Q*-switching elements in a pulsed ruby-laser system. Because of its highly regular nature, Birnbaum attributed this structure to diffraction effects associated with optical elements. Since then similar patterns have been produced in many semiconductors,[5–10] metals,[11–14] and dielectrics[15] using many different continuous and pulsed laser sources. It is doubtful if any researcher who has used high-intensity lasers for some time has not observed this effect, directly or indirectly. Some explanations of this phenomenon have centered on material properties. For example, suggestions have been put forward involving laser–acoustic-mode coupling,[7] driven surface plasmons,[13] or even Bose-Einstein condensation of bulk plasmons.[16] In specific cases it is possible that one or more of these mechanisms may contribute to the observed effect,

but it is doubtful that they can explain the universality of this phenomenon as it relates to different materials. This is particularly true since, if a linearly polarized excitation beam impinges on the material at normal incidence, the pattern of "fringes" has a spacing which, for metals and semiconductors, equals the wavelength of light, λ, and the orientation is perpendicular to the polarization of the beam. Because of these latter two properties, it is generally felt that the effect is due to an inhomogeneous energy deposition which occurs as a result of the interference of the incident beam with a "surface-scattered wave." This wave is considered to emanate from a surface point defect or a scratch. In fact, if the surface has a scratch which is oriented normal to the polarization of a p-polarized beam, two sets of fringes parallel to the scratch and of spacing $\lambda(1+\sin\theta)^{-1}$ and $\lambda(1-\sin\theta)^{-1}$ are observed, where θ is the angle of incidence of the beam. Although the simple "surface-scattered wave" picture is able to predict these results,[8] in the preceding paper[17] we have criticized the fundamental basis of this approach since the "surface-scattered wave" cannot satisfy Maxwell's equations. The simple approach also cannot account for the fact that, for normal incidence beams, the fringe spacing is observed to be λ for some materials but λ/n, for other materials, where n is the refractive index. An example of the former is GaAs at 1.06 μm,[10] while an example of the latter is NaCl at 10.6 μm.[15] Finally, the simple "surface-scattered wave" picture cannot explain the dependence of the fringe patterns on the polarization of the incident light.

In the preceding paper we have developed a first-principles theory which takes into account the details of the interaction of an electromagnetic wave with the microscopically rough selvedge of a surface. It shows that interference patterns can be generated, under certain conditions, which have the same spacing as those predicted by the "surface-scattered wave" model. The importance to this model of nonradiative "radiation remnants," selvedge structure, surface dielectric enhancement, and bulk dielectric constant have clearly been pointed out. It was also noted, as had been pointed out by Temple and Soileau,[15] that feedback would likely be a key factor in a complete theory. The theory predicts that the periodic surface damage can be produced in the vicinity of defects, however, a microscopically rough, albeit macroscopically smooth, surface is sufficient for the damage to occur. From the theory it is also clear that the surface damage is much more complex than has been previously realized, since fringe systems of various orientations and spacings can be produced at different angles of incidence and for different polarizations.

To our knowledge there has, as yet, been no detailed experimental investigation of either the damage patterns produced by beams of different polarizations and angles of incidence, or of the damage mechanisms themselves. In an earlier Letter,[18] we reported preliminary results on the damage patterns produced by 1.06-μm beams interacting with polished germanium samples. Because the damage patterns appear, in general, to be quite complex as observed through an optical microscope, we pointed out that it is more fruitful and certainly simpler to study the damage patterns in Fourier space by observing the far-field diffraction pattern of a cw laser reflected from the surface. This simple technique has proven to be extremely powerful in that it presents a great deal of previously unappreciated information on the surface damage in a neat, compact form.

In this paper we present the results of a more detailed investigation of laser-induced periodic surface structure (LIPSS) on different semiconductors and metals which are opaque at the wavelengths considered. We defer to a future publication similar phenomena in transparent dielectric media. In Sec. II we present a summary of the experimental apparatus, techniques, and surface preparation details that relate to our investigations. In Sec. III we present experimental results of the damage patterns on silicon, germanium, aluminum, and brass as induced by 1.06- and 0.53-μm radiation. The damage patterns are observed both in real and Fourier space, for s- and p-polarized beams at different angles of incidence. Our results indicate that, although the patterns differ in some details which are noted later, they have many common characteristics. In addition, all of the patterns can be explained in terms of the generalized surface-scattering model presented in the previous theoretical paper. Although the present paper is mainly concerned with the damage patterns produced and not with the dynamics of their formation during the laser pulse, in Sec. IV we present some results concerning the evolution of the LIPSS, on a shot-to-shot basis, for 1.06-μm light interacting with germanium. Although LIPSS can be produced with a single laser pulse, as many as 30 laser shots are required to establish a distinctive and shot-independent set of fringes over the entire beam cross section. During the first few shots, therefore, there clearly exists both temporal and spatial evolutionary processes which reinforce our assertions that feedback is an essential ingredient in any complete theory. In Sec. IV we also examine the role of scratches in influencing the damage evolution. Although the theory presented in the preceding paper is not complete in that it neglects feedback and employs a simple model for surface microroughness,

we find that the majority of our results can be explained by the theory. This applies not only to the shapes of the diffraction patterns produced but also to the relative intensities observed in these patterns, and to many of the qualitative aspects of the shot-to-shot evolution. A comparison of our theory and experimental results is presented in Sec. V. The paper concludes with a summary of our results on this intriguing universal damage phenomenon as well as directions for future research.

II. EXPERIMENTAL TECHNIQUES

The damage investigations reported in this paper were mainly carried out using the output of a Q-switched Quantel model 418A oscillator-amplifier Nd:YAG laser which produces 1.06-μm-fundamental and 0.53-μm—second-harmonic beams. The oscillator section is an unstable resonator which yields a nearly square spatial intensity profile for the pulse whose width is approximately 20 nsec. A Q-switched multimode Nd:glass oscillator with pulsewidths between 80 and 200 nsec produced similar damage results at 1.06 μm. In both cases the laser beams were linearly polarized. Fluence levels of the laser beams were measured using a Scientech energy meter. A Nomarski phase contrast microscope with a maximum magnification of 650× allowed the surfaces to be viewed in real space while a backreflection geometry, as illustrated in Fig. 1, provided a simple means of observing the Fourier transform (Fraunhofer diffraction pattern) of the surface. A cw argon-ion laser, used to obtain the diffraction patterns, was tuned to the shortest-wavelength line (0.46 μm) to resolve the finest structure possible on the surface.

Single-crystal and polycrystalline intrinsic Ge and Si were used in the studies, along with brass and aluminum which were obtained from stock. Different combinations of handpolishing, with and without chemical etches were used to prepare the surfaces. The polishing was done with either diamond paste or alumina powder with grit size down to $\frac{1}{4}$ μm. Standard CP-4A solution was used to etch Ge with NaOH being used on Si. Table I lists some relevant optical properties and the melting temperatures of the materials investigated.

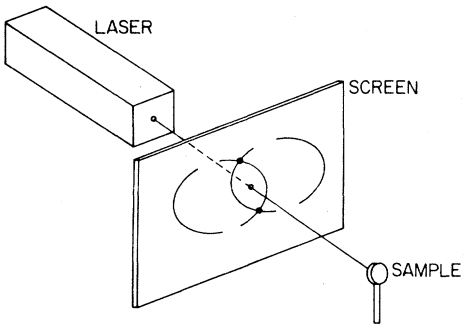

FIG. 1. Schematic diagram of the backreflection geometry used to view the diffraction patterns. A cw argon-ion laser operated on the 458-nm line was used as the source.

III. STEADY-STATE DAMAGE PATTERNS

In general, damage fringes can be produced with a single laser pulse, although the patterns develop further for successive laser shots. Initially, for a fluence which is just above threshold for damage, the fringes appear, but only where the most intense portions of the beam impinge on the surface. At higher fluences, the fringes form first in an annular region about the entire beam. Upon further irradiation they propagate inward to fill the entire beam cross section. In all cases, if the fluence is not too far above the periodic damage threshold, a steady-state structure develops after a large (typically >30) number of shots. In this section we confine our discussion to the steady-state patterns produced with 1.06-μm radiation incident on the four materials.

Since Ge under 1.06-μm illumination produces the most highly visible damage patterns, we initially restrict our discussion to this material. For p-polarized light at near-normal incidence on a nominally smooth Ge surface, the damage, as observed under a microscope, consists of two superimposed sets of fringes perpendicular to the polarization with spacing of $1.06/(1\pm\sin\theta)$ μm. We refer to these types of fringes as s^+ and s^- fringes. As θ increases, the fringes become less distinct as viewed under the microscope. However, for $\theta > 35°$ an extremely well-defined set of lines appears, with a spacing of $1.06/\cos\theta$ μm but which are parallel to the polarization. We refer to these as type-c fringes. Pictures of the type-c fringes for two different magnifications are shown in Fig. 2. Extremely uniform

TABLE I. Material parameters (see Ref. 19). Refractive indices ($n = n' + in''$), reflectivities at normal incidence (R), and melting temperatures (T_m) of target materials at wavelengths of interest.

Material	n'	n''	R	T_m (°C)
Aluminum (1.06 μm)	1.8	9.3	0.92	660
Aluminum (0.53 μm)	0.8	5.9	0.92	
Germanium (1.06 μm)	4.0	0.1	0.37	937
Germanium (0.53 μm)	5.2	2.2	0.51	
Silicon (1.06 μm)	3.5	10^{-4}	0.31	1410
Silicon (0.53 μm)	4.1	0.1	0.36	
Brass				

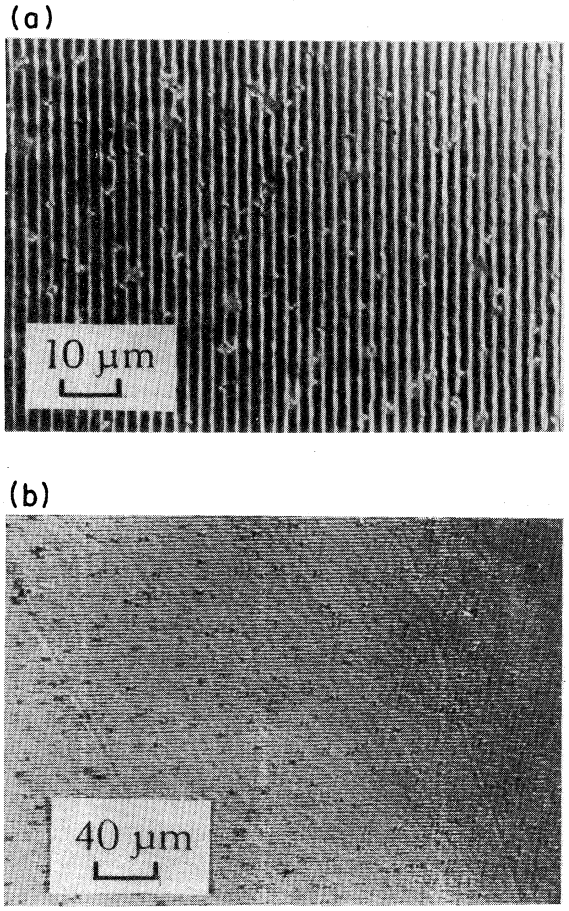

FIG. 2. Photographs of the strong type-c fringes produced in Ge with p-polarized light incident at an angle of 60°. The magnification in (a) is 4× that of (b).

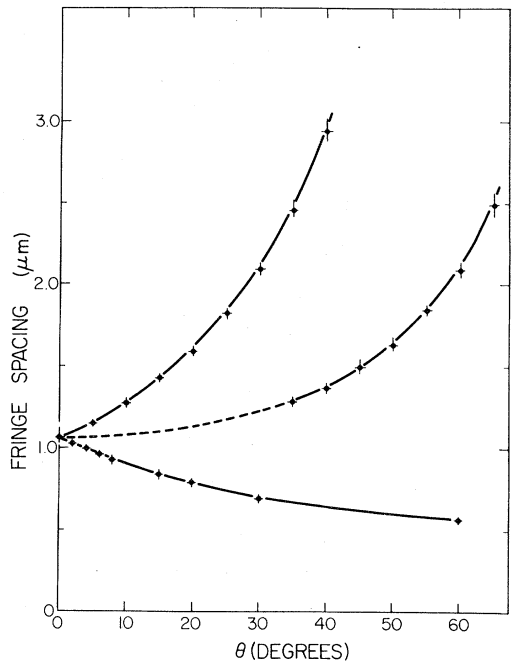

FIG. 3. Measured spacings of the dominant fringe patterns produced on Ge with p-polarized radiation as a function of θ, the angle of incidence. The curves are plots of the functions $1.06/(1-\sin\theta)$ (top), $1.06/\cos\theta$ (middle), and $1.06/(1+\sin\theta)$ (bottom).

fringes of this type can be produced over areas >1 cm^2. Figure 3 shows a plot of the measured spacings of the three different types of fringes with the solid lines representing the suggested angular dependences. For p-polarized light the threshold fluence required to produce periodic surface damage increases slightly with angle of incidence from 50 to 60 mJ/cm^2 as θ increases from 0° to 60°. For fluence levels between threshold and 100 mJ/cm^2 a steady-state pattern is developed after $\sim$30 shots. Fluence levels greater than $\sim$100 mJ/cm^2 produce good fringes after 30 shots but further irradiation causes the pattern to deteriorate. For fluence levels greater than $\sim$500 mJ/cm^2 the surface anneals to a very smooth finish in the central region with fringes formed in a narrow band around the perimeter where the local fluence is lower.

For s-polarized light, as θ is increased from 0°, the damage pattern is dominated by a single set of fringes running perpendicular to the polarization with a spacing of $1.06/\cos\theta$ μm. For $\theta>35°$, two sets of fringes form a cross-hatched pattern which is symmetric about the polarization axis, but neither of the fringe sets is perpendicular or parallel to it. The spacings of the fringes have no simple dependence on θ. The threshold fluence, 130 mJ/cm^2, required to produce damage with s-polarized light at 60° is more than twice the corresponding value for p-polarized light. Part of this increase can be understood in terms of the larger reflectivity for s-polarized light.

For nominally smooth surfaces which can be best characterized by a random microroughness, the $s^{\pm}$ fringes are observed over the entire surface. Viewed in terms of a "surface-scattered wave" model,[5] the fact that these type fringes dominate for p-polarized light at small angles of incidence indicates that the incident beam preferentially scatters in the forward and backward directions from the randomly rough surface. One might have expected that, for an isotropic surface, the incident beam would scatter in all directions across the surface. The appearance of the strong fringes running parallel to the plane of incidence for the case of p-polarized light at large angles of incidence indicates that, under these cir-

cumstances, the beam preferentially scatters along the surface at a nonzero angle with respect to the plane of incidence. In general, an incident beam characterized by the component of its wave vector in the plane of the surface, $\vec{\kappa}_i$, could produce surface-scattered waves described by a wave vector $\vec{\kappa}_s$, where $|\vec{\kappa}_s| = 2\pi/\lambda \equiv \tilde{\omega}$ and $\vec{\kappa}_s$ can be oriented in any direction parallel to the surface. The interference between the incident wave and the surface-scattered wave would be characterized by wave vectors $\vec{\kappa} = \pm(\vec{\kappa}_i - \vec{\kappa}_s)$, or

$$|\vec{\kappa}_i \pm \vec{\kappa}| = \tilde{\omega} . \quad (1)$$

If the beam is strong enough that the peak intensities in the interference pattern exceed the damage threshold of the material, the actual damage patterns observed for a given wavelength, polarization, angle of incidence, and surface condition then provide a mapping of the relative strength with which the incident beam scatters in any given direction across that surface.

Although it is difficult to quantitatively estimate the "amount of damage" related to any given fringe pattern by observation in real space, this information is conveniently obtained by measuring the relative intensities in the Fourier transform or diffraction pattern produced by reflection of a cw laser beam from the damaged area. The damage patterns produced with 1.06-μm, p-polarized light incident on a Ge surface at angles of incidence of 0°, 30°, and 60°, are shown in real space in Fig. 4. The corresponding diffraction patterns are shown in Fig. 5. It is apparent that for all angles of incidence the diffraction patterns do not correspond to discrete spots, as would be expected if the damage patterns merely consisted of a series of lines. Note, in the $\theta = 60°$ case, however, the strong dots in the diffraction patterns which occur at the intersections of the curves. These correspond to the dominant type-c fringes mentioned above. Figure 6 shows photographs of the diffraction patterns obtained using s-polarized light incident at 30° and 60°, respectively. A schematic summary of the damage patterns in Fourier space, observed using 1.06-μm radiation on Ge at various angles of incidence for both p- and s-polarized light, appears in Fig. 7. Each pattern contains an underlying geometry consisting of two overlapping circles of radius $2\pi/\lambda$, centered at $\pm(2\pi/\lambda)\sin\theta$ as predicted by Eq. (1). The extent to which these circles are filled out depends on the efficacy factor η (see preceding paper), which is associated with the efficiency of producing a scattered wave at $\vec{\kappa}_s$. This is discussed further in Sec. V. From Figs. 4–7, however, it is clear that the diffraction patterns are much richer, and potentially easier to understand than the actual damage patterns themselves. We note that the actual Fourier transform of the surface damage consists of overlapping *circles*. The diffraction patterns observed using the geometry of Fig. 1 are not circles because the spatial frequencies of a Fraunhofer diffraction pat-

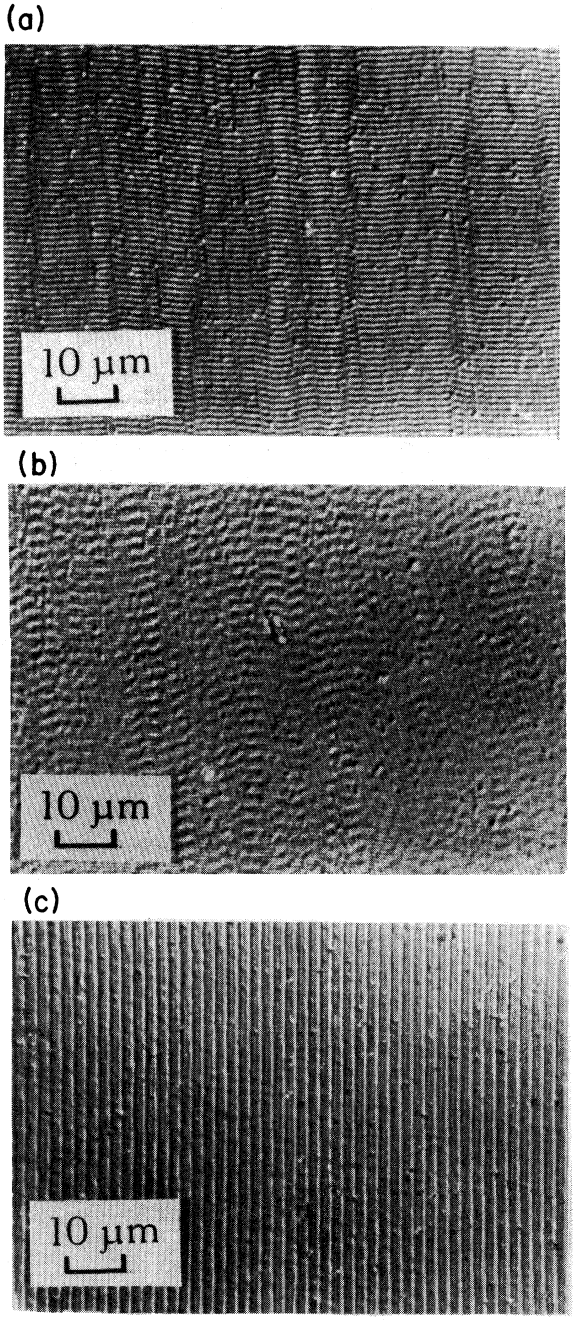

FIG. 4. Photographs of the surface structure produced on Ge with p-polarized 1.06-μm radiation incident at angles of (a) 0°, (b) 30°, and (c) 60°. Close inspection of (b) reveals both the type-s^+ and -s^- fringe patterns.

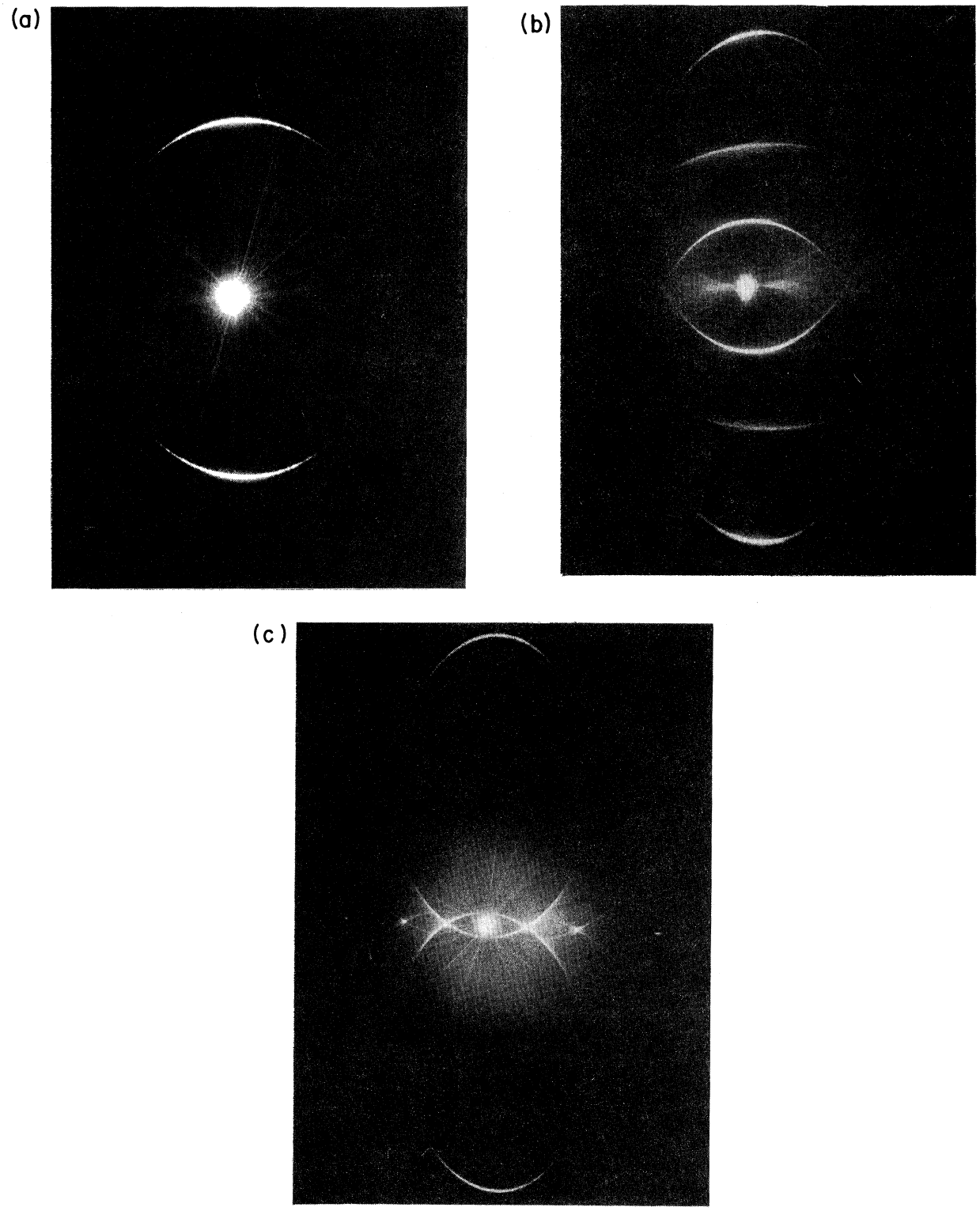

FIG. 5. Photographs of the diffraction patterns produced on the screen of Fig. 1 from the samples shown in Figs. 4(a), 4(b), and 4(c) are shown in (a), (b), and (c), respectively. Note that all photographs of the diffraction patterns were taken at an angle with respect to the screen which introduces some distortion.

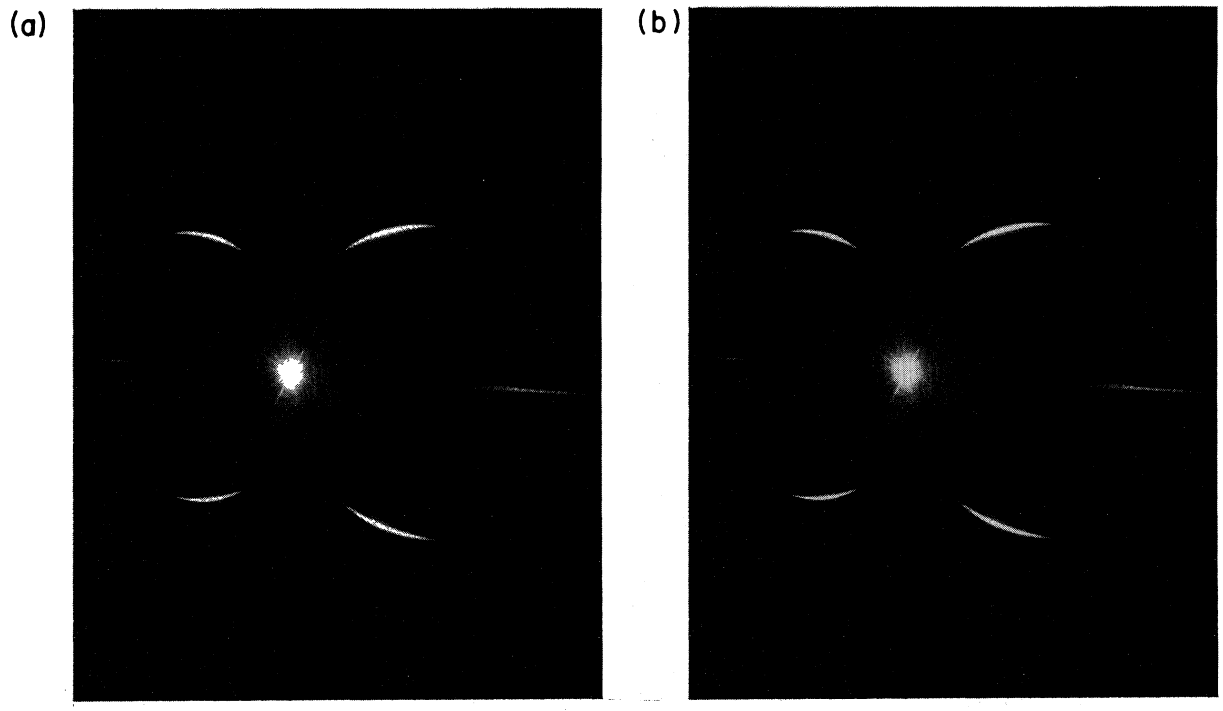

FIG. 6. Photographs of diffraction patterns produced by Ge samples which were irradiated with s-polarized 1.06-μm radiation incident at (a) 30° and (b) 60°.

tern are not exactly the same as the Fourier components of the diffracting object and because the diffraction patterns are projected onto a plane. Attention is also drawn to the fact that several photos show second-order diffraction effects. The diffraction patterns of the steady-state damage regions do not depend significantly on whether the surface was polished or polished and etched. Figure 8 illustrates the regions of the diffraction patterns which we now, in a generalization of our previous definitions, refer to as type-s^+, -s^-, and -c fringes.

Silicon under 0.53-μm illumination yields results

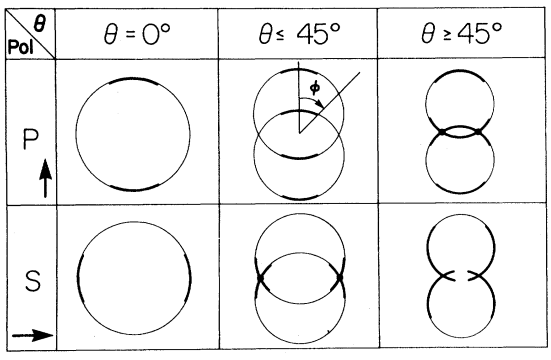

FIG. 7. A table summarizing the general trend of the Fourier transform of the damage structure observed on Ge at 1.06 μm, as a function of θ and polarization.

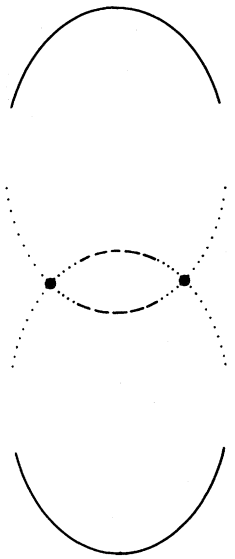

FIG. 8. Type-s^+, -s^-, and -c fringes mentioned in the text refer to those which contribute to the solid, dashed, and dotted portions of the diffraction pattern, respectively.

very similar to that of Ge at 1.06 μm with respect to the ease of formation and visibility of the fringe patterns produced. This is not surprising since the absorption coefficients appropriate to the two situations are similar (cf. Table I). Fringe patterns can also be generated on Al and brass with both 1.06- and 0.53-μm radiation although a much higher threshold intensity is required and the range of intensities over which this occurs is much smaller than that referred to above. The higher fluence threshold is partially explained by the larger reflectivity ($\sim$0.92) of the metals compared to that ($\sim$0.3) of the semiconductors.

Since the diffraction patterns produced by the damaged surfaces provide a simple quantitative measure of the relative efficiency for an incident beam to produce damage with various Fourier components, it is of interest to compare the patterns produced on different surfaces for different λ. The diffraction patterns from the damaged surfaces of Al irradiated at 0°, 30°, and 60° for 1.06- and 0.53-μm p-polarized light are shown in Figs. 9 and 10, respectively. Figure 11 shows the diffraction patterns from Ge irradiated at 0.53 μm for 0°, 30°, and 60°. (Note that with 0.53-μm radiation the spacing of the type-s^+ fringes can be less than the wavelength of the Ar-ion laser used to make the diffraction patterns and therefore the diffraction patterns for 0.53-μm illumination only represent the more widely spaced ripple pattern actually on the surface.) The same underlying patterns are observed for both 1.06-μm and 0.53-μm radiation incident on Si and brass. The differences that do exist relate to the degree to which the underlying intersecting circle patterns are filled out in the actual diffraction pattern. The most obvious difference is that we observe no exceptionally bright dots in the patterns of Si, Al, or brass at any angle of incidence indicating that the type-c fringes appear to be extremely noticeable in Ge only. (Note also that type-c fringes exist as strong dots in the diffraction patterns for Ge with both 1.06- and 0.53-μm radiation.) The type-s^- fringes are stronger in Al than in any other material at both wavelengths. The curves which make up the diffraction patterns in brass are much broader and more diffuse than in the other materials indicating that the spacing of the fringes oriented in any given direction is not precisely defined. Aside from the lack of type-c fringes, Si is quite similar to Ge. In all materials the threshold for s-polarized fringe formation is much larger than that for p polarization: In fact, we could not produce fringes in Si with s-polarized, 1.06-μm radiation. However, even for p-polarized light, the fringes in Si were very weak. This is somewhat expected since the absorption coefficient of silicon at 1.06 μm is quite small.

IV. SHOT-TO-SHOT EVOLUTION OF THE DAMAGE PATTERN

As indicated above, the damage evolves both spatially and temporally for the first 20—30 laser shots. In order to study these dynamic aspects of fringe formation we conducted two experiments. In the first, a polished, but not etched, sample of Ge was placed directly on the stage of the Nomarski microscope and then irradiated by the Nd:YAG laser. In this way a single portion of the surface was viewed in real space on a shot-to-shot basis. In a second, similar experiment a 3.5-cm diameter Ge sample was mounted on an x-y translation stage and different spots were illuminated with different numbers of 1.06-μm-laser pulses. The resulting patterns could then be viewed in both real and $\vec{\kappa}$ spaces.

At normal incidence with a fluence of $\sim$100 mJ/cm^2 the fringes appear after a single laser pulse but only in a narrow annular region around the perimeter of the beam. On scanning the focused Ar^+ beam across the illuminated region we observe that outside the annular region the diffraction pattern consists only of diffuse scattering from the random scratches left on the surface from polishing. For the cw beam incident on the annular region, this diffuse background has superimposed on it the characteristic partially completed circular pattern as shown in Fig. 5(a). Inside the annular region there are no signs of any circular pattern corresponding to the fringes; however, the diffuse background is much reduced. In real space this observation corresponds to the fact that the surface appears smoothed, indicating that it is, in some sense, melting uniformly. Following pulses cause the annular region to grow towards the center while the central region begins to develop (1—3)-μm-diameter pits. After 30 pulses, the entire surface is covered with fringes which remain unless the intensity is greater than $\sim$100 mJ/cm^2 in which case further illumination causes the central region to develop very deep fringes which eventually collapse, leaving a mottled, irregularly damaged area. It is interesting to note that even after the steady-state pattern is achieved, a narrow annular ring around the perimeter of the damaged area is still discernable to the naked eye when the area is viewed at a glancing angle. No demarcation is observed when the area is viewed at normal incidence. We believe this is due to the fact that, as is discernible under the microscope, the fringes in the annular region have a different depth profile than those in the central region. We suggest that this occurs since in the annular region the Ge actually only melts along narrow lines while in the central region the whole surface melts, the fringes appearing there because certain regions melt more dee-

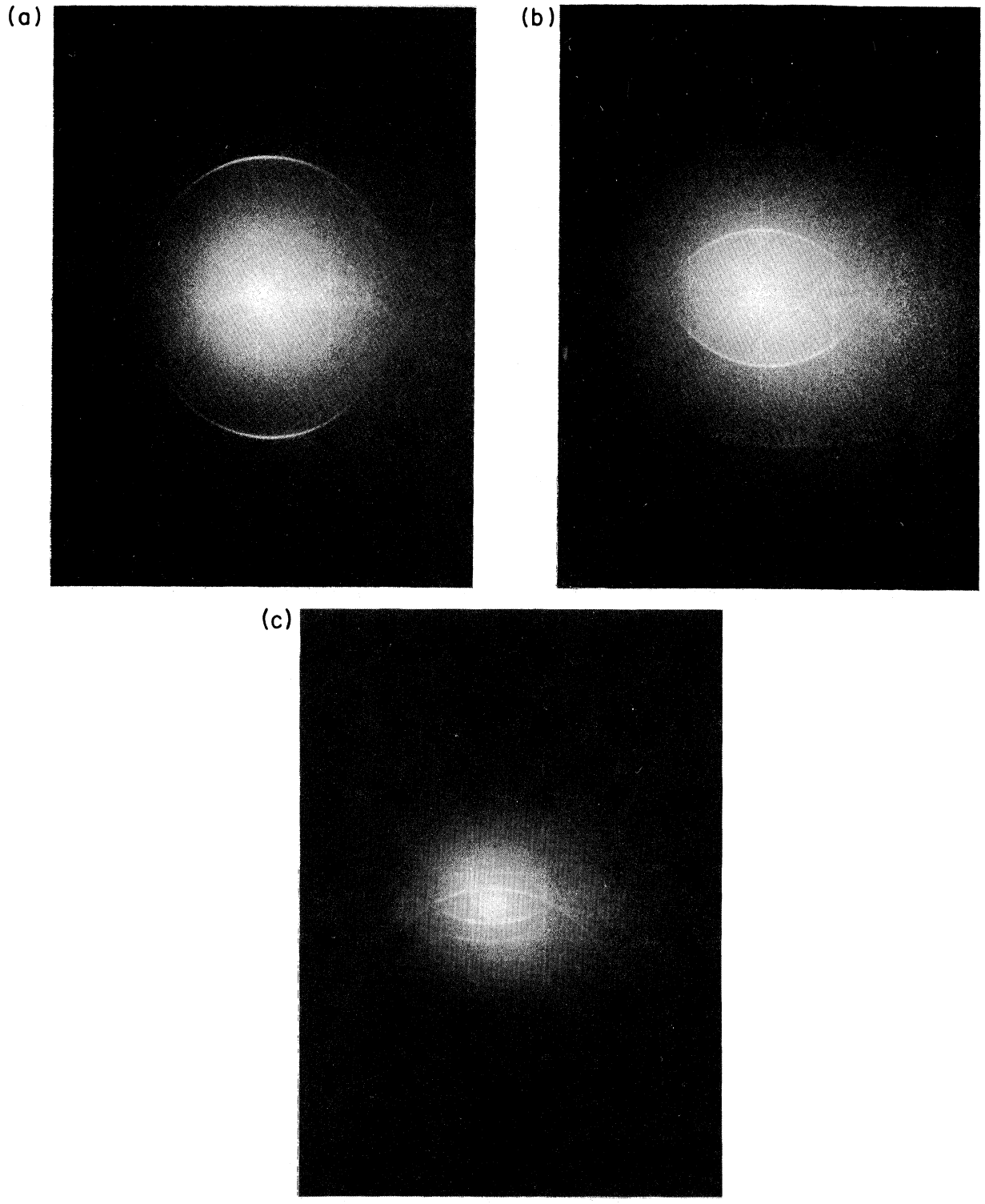

FIG. 9. Diffraction patterns produced from Al irradiated with p-polarized, 1.06-μm radiation incident at (a) 0°, (b) 30°, and (c) 60°.

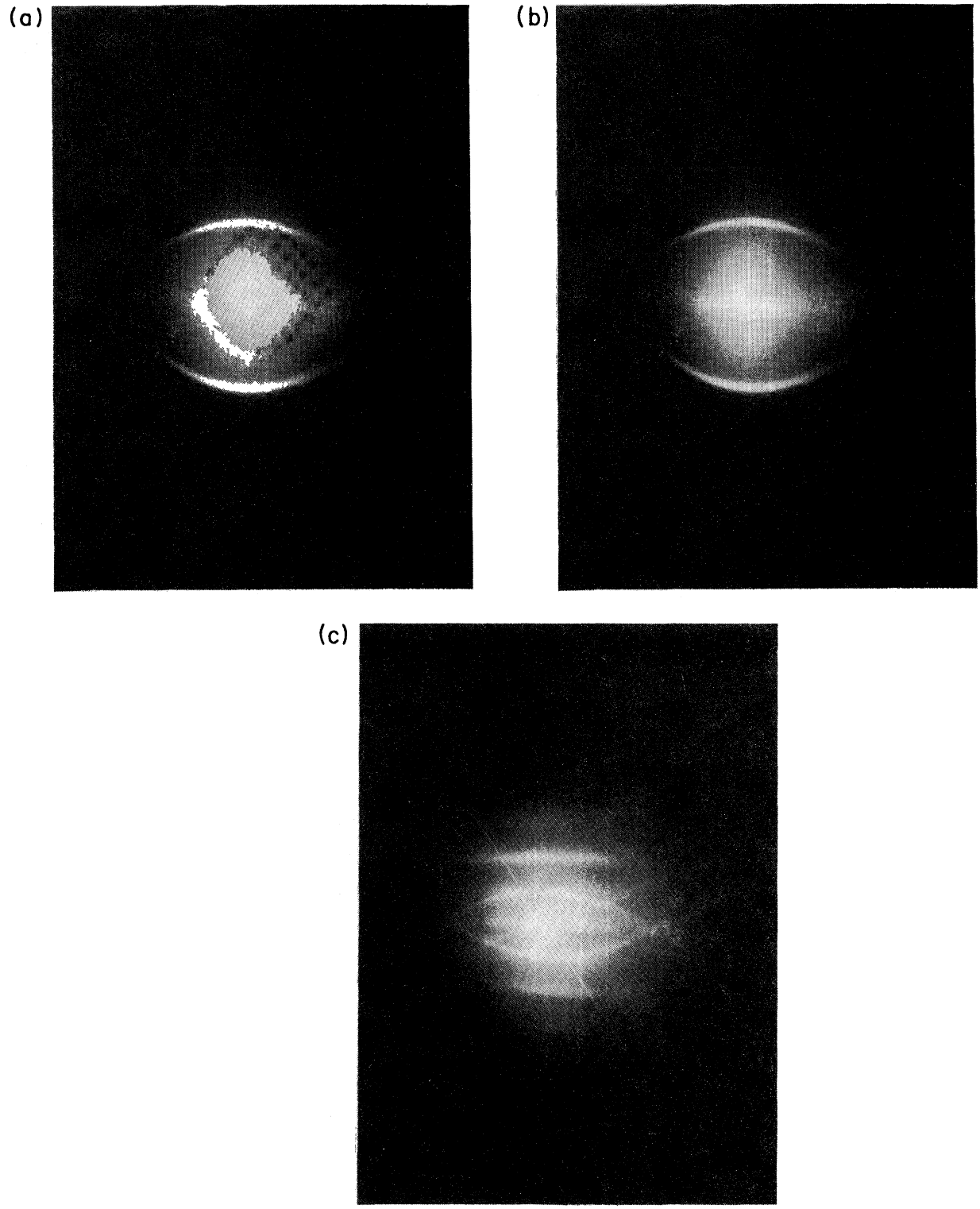

FIG. 10. Diffraction patterns produced from Al irradiated by p-polarized, 0.53-μm radiation incident at (a) 0°, (b) 30°, and (c) 60°. The shadow is that of the sample in a holder.

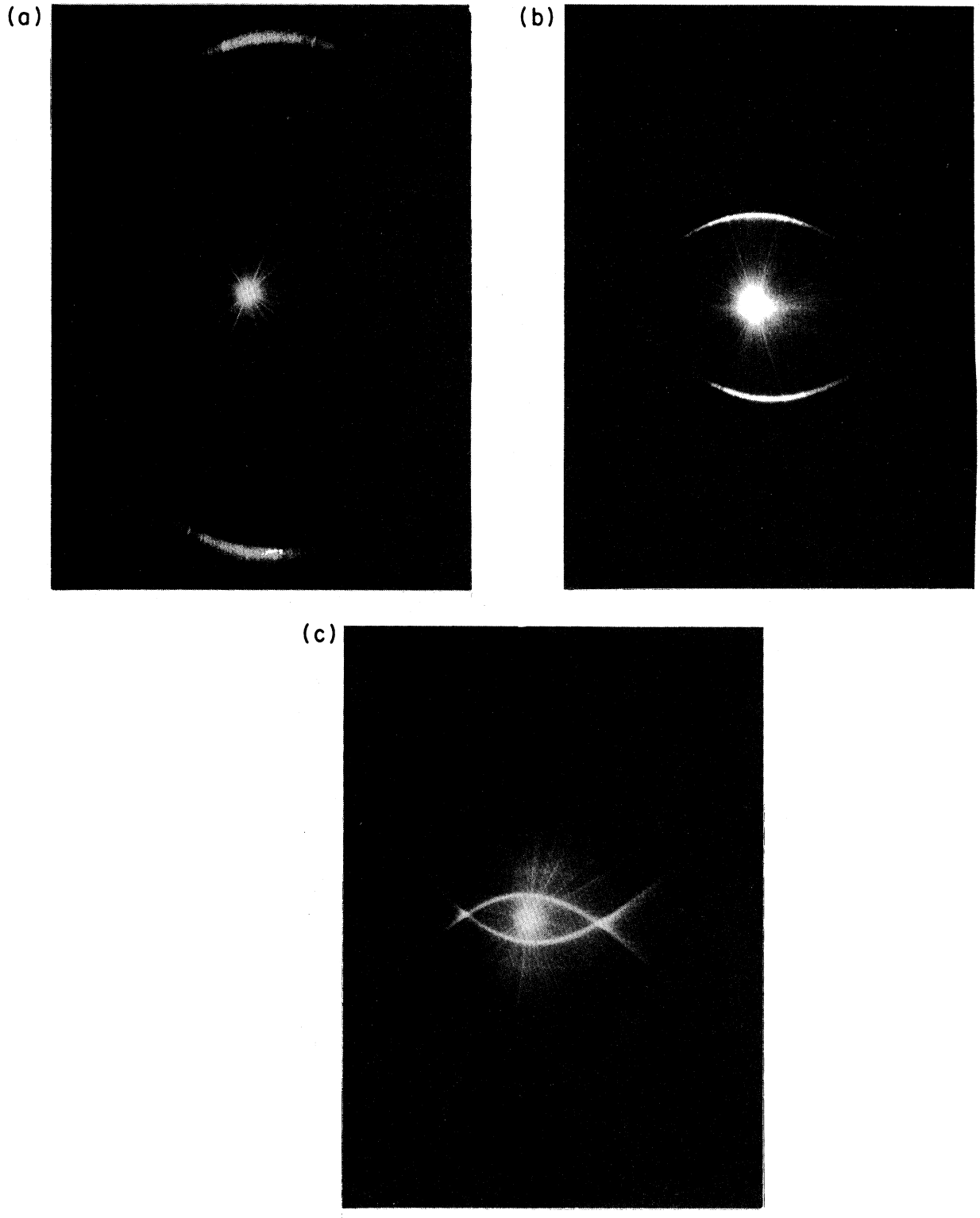

FIG. 11. Diffraction patterns produced from Ge irradiated by p-polarized, 0.53-μm radiation incident at (a) 0°, (b) 30°, and (c) 60°.

ply than others. As the intensity is increased the diameter of the annular region increases in a manner similar to the way the annular amorphous ring observed in laser annealing of Si by Liu *et al.*[20] changes with intensity.

The evolution observed when the laser pulses are incident at large ($>35°$) angles is more interesting than for $\theta=0°$ since all three types of fringes appear at different stages in different portions of the illuminated region. At an incident fluence of 100 mJ/cm^2, the first sign of fringes occurs after two laser pulses have hit the sample but, as at normal incidence, they are confined to a narrow annular region surrounding the central hot portion of the beam. There are only type-s^+ fringes at this stage: Absolutely no indication of either type-c or type-s^- fringes appear until the surface has been hit by at least eight laser pulses. As at normal incidence, the central region appears smoothed over with small pits developing before fringes form there. From 2 to 8 shots the type-s^+ fringes in the annular region extend towards the center. After eight shots, strong peaks begin to appear in the diffraction pattern from the annular region indicating type-c fringes are forming on top of the type-s^+ ones already there. Subsequent irradiation with laser pulses simultaneously causes the diffraction pattern in the annular region to fill out [cf. Fig. 5(c)] and fringe formation propagates inward to eventually fill the illuminated region. The precise intensity distribution of the diffracted light in the final steady-state pattern depends upon the 1.06-μm pulse fluence. If the fluence is too large ($\gtrsim 200$ mJ/cm^2) the type-s^- ripples tend to grow rapidly and ultimately dominate the damage pattern. As at normal incidence, fluence levels greater than 500 mJ/cm^2 anneal the surface, leaving only a narrow ring of fringes around the perimeter of the central region. This ring actually consists of three concentric rings. The innermost one consists of type-s^- fringes, the middle ring is made up of type-c fringes while the outermost annulus has predominantly type-s^+ fringes.

One final observation concerns the role of scratches and defects on the evolution of the fringe patterns. The only obvious difference between the damage produced in polished versus polished-then-etched samples is that during the early stages of development (<30 shots) the diffraction patterns from the polished surfaces contain bright spots while those from the etched surfaces are smoothly varying. We purposely scratched the samples in a discrete number of directions and performed the shot-to-shot experiments described above. If the purposely placed scratches are sufficiently shallow the fringes first form parallel to these scratches, but eventually the scratches are smoothed over and the regular smooth diffraction pattern develops. Figure 12 is a photograph of the diffraction pattern at an early stage of development for a Ge sample preferentially scratched in various directions with 3-μm diamond paste. Note that the randomly spaced scratches produce radial lines in the diffraction patterns which are perpendicular to the scratch orientation. Note also that the bright spots in the fringe diffraction pattern appear at the intersection of the usual fringe diffraction pattern and the radial lines from the scratches. If the final polish of the entire sample is done with 6-μm grit diamond paste, no fringes are formed until the 1.06-μm pulses have partially smoothed out the rough surface at which point the regular evolutionary process commences. If the surface is treated only with fine emory cloth (#600), no fringes are formed. This indicates that very rough surfaces will not give rise to the periodic damage structure.

With the use of the microscope to observe the surface after 10 to 12 shots it is possible to capture the

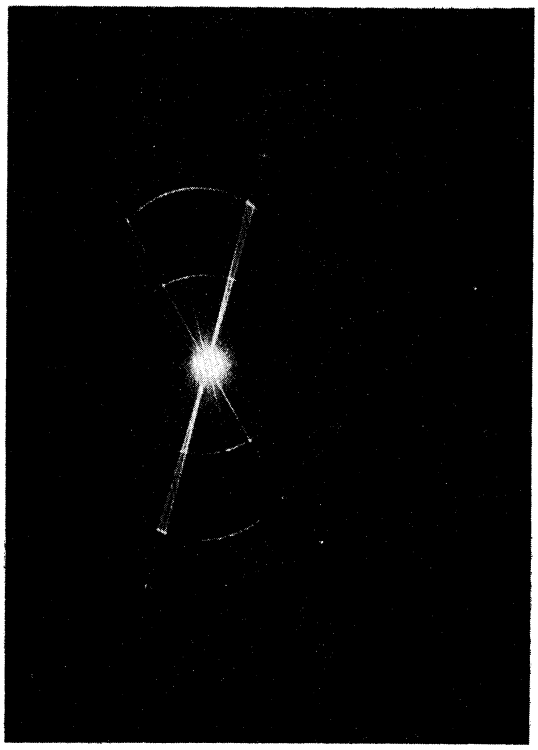

FIG. 12. Diffraction pattern produced from a Ge surface preferentially scratched in a number of discrete directions prior to irradiation by five shots of p-polarized 1.06-μm radiation incident at 15°. Note the radial lines corresponding to the diffraction from the randomly spaced, but nearly parallel scratches. Note also the bright spots at the intersections of these radial lines with the "usual" fringe diffraction pattern.

beginning stages of the formation of the type-*c* fringes. It appears as if the large expanses of parallel lines shown in Fig. 5 originate at small localized defects as the photograph in Fig. 13 illustrates. At this critical stage of development the surface is covered with many localized defects which seem to be produced by the action of the initial laser pulses on the sample surface. Fanlike ripple patterns extend from these localized defects but further irradiation causes only a single Fourier component of this fan pattern to develop into the parallel type-*c* fringes. Careful inspection of Fig. 13 reveals the continuous transformation from the fan to the parallel line structures. At higher laser intensities it is difficult to observe this stage of development, presumably because the transformation from the fan to the linear pattern occurs to a greater extent during a single laser pulse.

V. COMPARISON OF THEORY AND EXPERIMENT

In the preceding paper a theory was presented which describes the electric-field-intensity distribution created by a plane wave incident on a thin, rough surface selvedge region, of height much less than λ, atop a bulk solid. The bulk material is characterized by its dielectric constant ϵ at the incident wavelength. The rough surface region in general has a dielectric constant which is different from that of the bulk, although all of the results referred to in this paper assume that the surface has the same dielectric constant as the bulk. The roughness in the surface region is itself characterized by two parameters. The first, called s, is the ratio of a typical correlation distance in the plane of the surface to the thickness of the selvedge (s corresponds to the shape of the "islands" which make up the surface). The second, called F, is the filling factor which represents the fraction of the surface filled up with "islands." The incident plane wave $\vec{E}_i$ is defined by a wave vector $\vec{k}$, $|\vec{k}| = 2\pi/\lambda = \tilde{\omega}$, the angle of incidence θ, and the polarization. Actually, it is only the component of the wave vector parallel to the surface $\vec{\kappa}_i$, $|\vec{\kappa}_i| = \tilde{\omega}\sin\theta$, which is of primary importance.

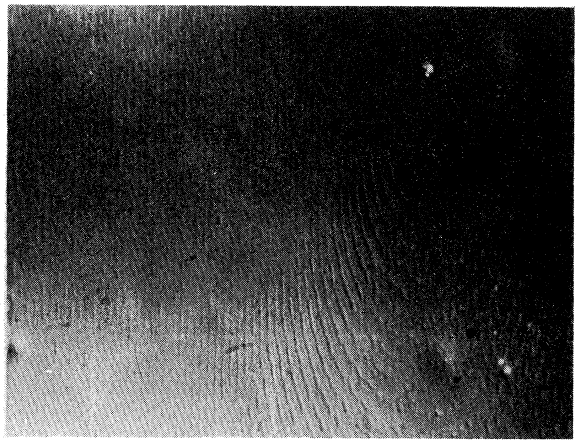

FIG. 13. Photograph of a portion of the Ge surface after being hit by 10 pulses Of 1.06-μm, *p*-polarized radiation. Note how the fanlike pattern emanating from the localized defect continuously transforms into the parallel, type-*c* fringes which eventually dominate.

With the use of a variational approach, the polarization induced in the selvedge region by the incident beam is calculated for a given set of parameters. The electric field produced by this induced polarization sheet is obtained and added to the normally refracted component of the incident beam to obtain the total field distribution just below the surface. The two-dimensional Fourier transform of the resulting intensity distribution is then written as the product of the Fourier component of the surface roughness at $\vec{\kappa}$, $b(\vec{\kappa})$, and an efficacy function $\eta(\vec{\kappa})$. For given s and F, a surface contains a wide range of Fourier components, $b(\vec{\kappa})$. Prior to sample irradiation this spectrum might be expected to vary slowly with $\vec{\kappa}$. However, for a given $\vec{\kappa}_i$, polarization, and selvedge parameters, η contains sharp peaks as a function of $\vec{\kappa}$ which are superimposed on a slowly varying background (see the sharp peak in Fig. 14 which is a plot of η vs $\vec{\kappa}$ for Ge with 1.06-μm, *p*-polarized light incident at $\theta = 60°$). In general, as pointed out in the preceding paper, the position of these peaks is in good agreement with Eq. (1). The theory thus suggests that when plane waves are incident on rough surfaces, the intensity of the field just below the surface is strongly modulated and its spatial Fourier transform contains strong peaks. Based on the premise that periodic damage is produced with Fourier components corresponding to the peaks in the intensity distribution, we compare the magnitudes and positions of the peaks in $\eta(\vec{\kappa})$ with the diffraction patterns observed experimentally. Clearly, since damage mechanisms are in general complex and nonlinear, one cannot expect complete quantitative agreement between the magnitudes of the inhomogeneous energy deposition and the "amount of damage" at any given wave vector. However, we find that very good semiquantitative agreement is achieved in the comparison.

The comparisons were carried out as follows. The bulk and selvedge dielectric constants were set equal to the bulk value at the incident wave length. One might think the logical treatment of the surface would be to experimentally measure the roughness

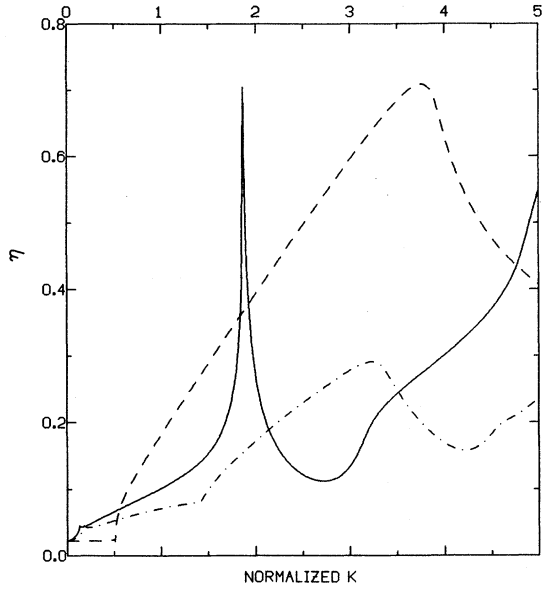

FIG. 14. η as a function of $\kappa/\tilde{\omega}$ for p-polarized light incident at 60° on a material with the optical properties of Ge at 1.06 μm ($n=4+i0.1$), with surface roughness characterized by $s=10$, $F=0.1$. Solid line: $\phi=0°$; dash-dots: $\phi=45°$; dash: $\phi=90°$. (See Fig. 7 for the definition of ϕ.)

parameters s and F of the prepared sample and insert these into the theory to calculate a $\eta(\vec{\kappa})$ to compare with the diffraction patterns. Aside from the fact that such a surface characterization is difficult to perform, as we shall argue below, the initial surface roughness characteristics are felt not to be important in determining the steady-state patterns obtained (see the discussion below). We therefore adopt a different and perhaps potentially more useful approach, fitting the surface parameters s and F to give the best agreement with the experimentally observed diffraction patterns. It is interesting to note that except for a factor independent of κ, *in the case of s-polarized light the theory predicts no dependence of* $\eta(\vec{\kappa})$ on s and F. Thus there are no parameters to be fitted in this case and in some sense the comparison for s-polarized excitation provides a more convincing test for the validity of our theory than does the p-polarized case. The comparison presented here is done for Ge using 1.06-μm radiation since these conditions lead to the best quality and most easily observed diffraction patterns.

The gross features of the diffraction pattern produced with 1.06-μm, p-polarized light incident at $\theta=60°$ on Ge [see Fig. 5(c)] can be summarized as follows. With reference to the inset in Fig. 17(a), the intensity is quite strong at $\phi=0°$ on the outermost portion of the circle and decreases to zero at $\phi\simeq45°$. Past $\phi\simeq45°$ the intensity rises, has a sharp maximum at $\phi=90°$, and remains bright from $\phi=90°$ to $\phi=180°$. In sharp contrast, for 1.06-μm, s-polarized light incident on Ge at 60° [see Fig. 6(b)] the diffraction pattern peaks at $\phi\simeq45°$ and shows a significant intensity only within a small range of $\pm10°$ near $\phi=45°$. Graphs of the efficacy factor $\eta(\vec{\kappa})$ corresponding to the above two excitation conditions are shown in Figs. 15 and 16. The three separate plots correspond to $\vec{\kappa}$ oriented at $\phi=0°$, 45°, and 90° (see Fig. 7). For the s-polarized case, only the $\phi=45°$ plot shows a strong indication of a peak, in agreement with the actual diffraction pattern in Fig. 6(b). For p-polarization, there is a single peak in the $\phi=90°$ plot, only an s^- peak in the $\phi=45°$ plot, and two peaks in the $\phi=0°$ case, again in agreement with the gross features of the pattern shown in Fig. 5(c). The s and F factors were set equal to 0.4 and 0.1, respectively, to obtain the plots of Fig. 15; roughly speaking, $s=\frac{5}{12}\simeq0.41$ corresponds to local-field corrections appropriate to "spherically shaped islands" (see preceding paper). Note that the plots in Fig. 14, which are also for p-polarized light incident at $\theta=60°$ on Ge but with $s=10.0$ and $F=0.1$, do not show the peak at $\phi=90°$ or the inside peak at $\phi=0°$. We thus conclude that the roughness on the Ge surface in the regions where damage is produced which gives rise to a diffraction

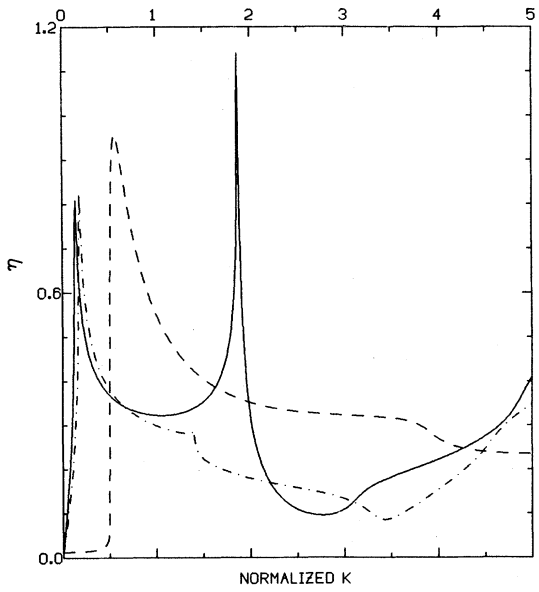

FIG. 15. η as a function of $\kappa/\tilde{\omega}$ for p-polarized light incident at 60° on a material with the optical properties of Ge at 1.06 μm ($n=4+i0.1$), with surface roughness characterized by $s=0.4$, $F=0.1$. Solid line: $\phi=0°$; dash-dots: $\phi=45°$; dash: $\phi=90°$. (See Fig. 7 for the definition of ϕ.)

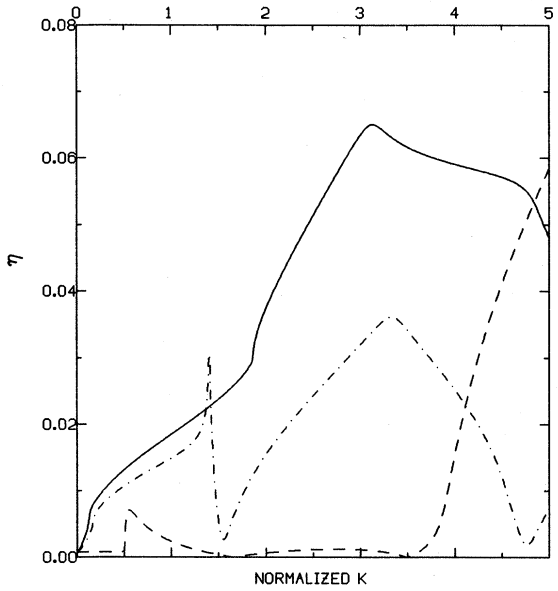

FIG. 16. η as a function of $\kappa/\tilde{\omega}$ for s-polarized light incident at 60° on a material with the optical properties of Ge at 1.06 μm ($n=4+i0.1$). The surface roughness parameters were set at $s=0.4$, $F=0.1$ (cf. Fig. 15), but for this polarization the shapes of the curves are independent of those parameters (see text). Solid line: $\phi=0°$; dash-dots: $\phi=45°$; dash: $\phi=90°$. (See Fig. 7 for the definition of ϕ.) The sharp peak at $\phi=45°$ is seen only at ϕ in the neighborhood of that and equivalent angles.

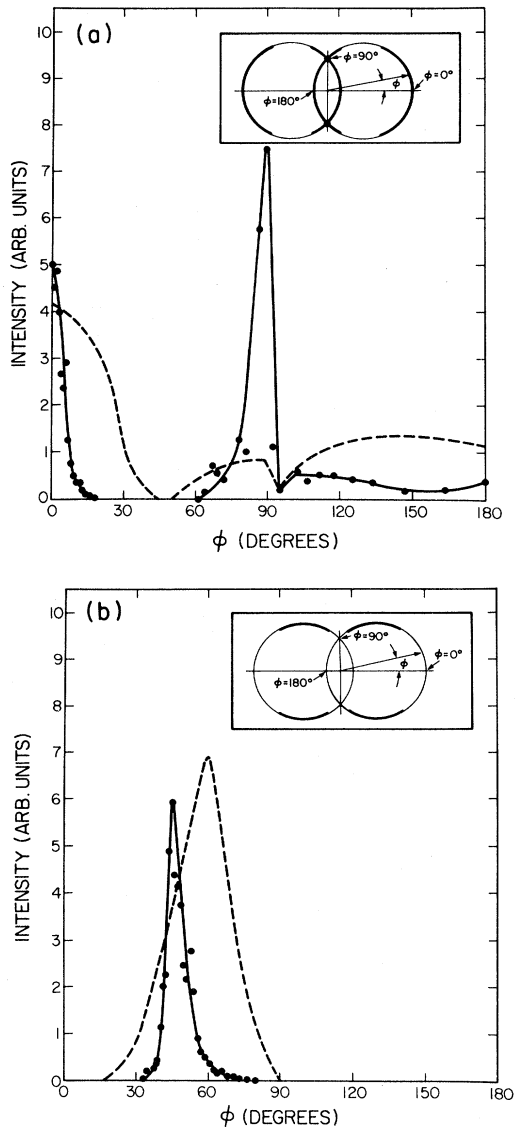

FIG. 17. Comparison of the theoretical and experimental intensity distributions in the diffraction patterns produced with 1.06-μm light incident on Ge at 60° for (a) p and (b) s polarizations. The insets show schematically the diffraction patterns and the angle ϕ against which the intensity has been plotted. The solid curve is a guide to the eye for the data; the dashed curve represents a theoretical result as explained in the text.

pattern, as in Fig. 5(c), is more aptly described as consisting of localized spherically shaped defects rather than pancakelike defects. This agrees with our observations of microscopic bubbles on the surface, the creation of which seems both theoretically and experimentally necessary to produce the type-c fringes.

In order to provide a more convincing comparison of the theory and experiment, the intensity in the Fraunhofer diffraction pattern was measured using a 1-cm^2 Si photodiode mounted on an x-y translation stage. A 5-mm-diam. aperture was placed in front of the detector to define an angular resolution of $\Delta\phi=0.5°$. Care was taken to keep the intensity within the linear response region of the photodiode. The data on the intensity distribution obtained as a function of ϕ for diffraction patterns from Ge samples irradiated with p- and s-polarized light at 60° incidence are shown in Figs. 17(a) and 17(b), respectively, with the solid lines being a guide to the eye. We stress that these are plots of the raw intensity measurements in the Fraunhofer plane, there have been no corrections made for scattering efficiency or the fact that not all points on the plane are equidistant from the scattering point. The gross features we wish to illustrate are unaffected by such scaling.

A difficulty arises, however, when one attempts to extract quantitative information about $\eta(\vec{\kappa})$ from the theory. Since many of the peaks in $\eta(\vec{\kappa})$ (see Fig. 15) ride upon significant backgrounds which are, in general, of different magnitudes on either side of the peak, the question arises as to how much

of the peak contributes to damage at that wave vector. Again we stress that there is no obvious direct connection between the degree of spatial inhomogeneity of intensity and the resulting damage at a given wave vector. We merely wish to demonstrate the fact that the gross features in the inhomogeneous intensity patterns as represented by the peaks in $\eta(\vec{\kappa})$ are quite similar to the experimentally observed diffraction patterns. With this in mind we estimated peak minus background values from plots such as in Fig. 15 done at 5° increments in ϕ, and the results for 1.06-μm, p- and s-polarized light on Ge at 60° angle of incidence are shown as dashed lines in Figs. 17(a) and 17(b). The p-polarized values were obtained using $s=0.4$ and $F=0.7$.

Except for the large spike in the experimental data at $\phi=90°$ for p-polarized light, the gross features of the theory and experiment are in good agreement. We chose the value $s=0.4$ simply because "spherical-like," rather than "pancakelike," islands of roughness seem necessary to lead to a prediction of any type-c fringes at all for a p-polarized damaging beam (cf. Figs. 14 and 15), and we chose $F=0.7$ to give good agreement between theory and experiment for the ratio of the magnitudes of s^+ and s^- fringes in Fig. 17(a). The large peak at $\phi=90°$, in the experimental results, corresponds to the strong type-c fringes which clearly are not as strongly peaked in our theory; this is true regardless of the values of s and F that are chosen. Recall, though, that the strong type-c fringes appear to be peculiar to Ge, and we suspect that feedback mechanisms are responsible for their dominance. We emphasize that the theoretical predictions for damage from an s-polarized beam (Fig. 17(b)] are, except for a factor that does not depend on $\vec{\kappa}$, independent of the values of s and F chosen; thus there are no adjustable parameters in the peak shape predicted in Fig. 17(b) and, remembering that no feedback effects are taken into account in our theory, we consider the agreement between theory and experiment demonstrated in Fig. 17(b) to be quite impressive. It is also interesting to note that the relative magnitudes of the peaks predicted for s- and p-polarized damaging beams (cf. Figs. 15 and 16) is in general agreement with the experimentally observed higher damage threshold for s-polarized light. For the sake of brevity we have only presented graphical comparisons of experiment and theory for a damaging beam incident at $\theta=60°$; similar agreement in the position of the peaks, and in the gross features of the intensity distributions, is obtained for other angles of incidence.

The only explicit wavelength and/or material dependence in the theory, which assumes the thickness of the roughness region is much less than the wavelength of light, resides in the dielectric constant and, implicitly, in the s and F factors. Calculations show that the predicted results are not critically dependent on the dielectric constant over quite a large range, and the predicted patterns for Si, Al, and brass are quite similar to those for Ge in many respects. Figure 18 shows a plot of $\eta(\vec{\kappa})$ for Al corresponding to that of Fig. 15 for Ge, using the same roughness parameters. Note that the peaks are much sharper, and that the type-c fringe peak at $\phi=90°$ in fact exhibits an interesting fine structure. Both these differences result from the fact that, in a metal with a large negative dielectric constant, the peaks correspond to the excitation of surface plasmons, rather than the generation of "radiation remnants," as has been discussed in the preceding paper. Thus there are important physical differences, between metals and semiconductors, in the electromagnetic field structures leading to periodic surface damage. Considering however, both the simplicity of the theory, and the gross comparison of theory with experiment that we are able to make, Figs. 15 and 18 are qualitatively very much the same. Since the observed diffraction patterns are also quite similar in the two cases, we are satisfied with the agreement between theory and experiment, in lieu of a more sophisticated model.

Returning to Ge, the fact that type-c fringes seem

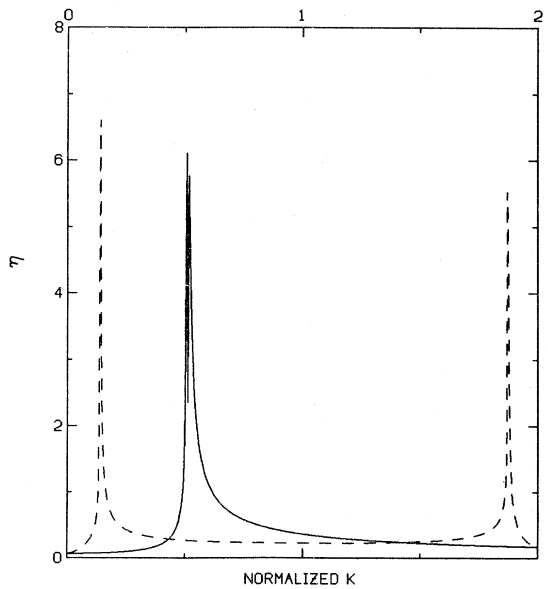

FIG. 18. η as a function of $\kappa/\bar{\omega}$ for p-polarized light incident at 60° on a material with the optical properties of Al at 1.06 μm ($n=1.8+i9.3$), with surface roughness characterized by $s=0.4$, $F=0.1$. Dashed line: $\phi=0°$; solid line: $\phi=90°$. (See Fig. 7 for the definition of ϕ.) Note the change in scale and legend from Figs. 14—16.

to require "spherelike" roughness (or in fact "bananalike" roughness with $s \ll 1$) is consistent with the experimental results and actually sheds light on the evolutionary process. The evolutionary process for the formation of these fringes could occur as follows. Consider a laser pulse with a central intensity large enough to uniformly melt a region of the surface. At some point away from the center the intensity must be just slightly below the damage threshold. However, we have seen that a rough surface can redistribute the energy and concentrate it in certain Fourier components. Therefore, even if the incident intensity is just below threshold, the peak intensity in the interference pattern could be above threshold and hence the surface would melt along localized lines only. If the intensity is too large, the sample melts the region between maxima in the interference pattern as well, and, if the spacing of the fringes is too small, the molten phase is not able to sustain the structure. The fact that only type-s^+ fringes form during the first few pulses in the annular region thus indicates that the initial surface roughness is better described as pancakelike rather than spherical-like (see Fig. 14 as opposed to Fig. 15). In the central region, the first few laser shots interact with the surface and cause defects and pits to form. This is likely the stage most sensitive to the wavelength and material properties, as evidenced by the fact that the type of defects formed in Si at 0.53 μm are completely different from those formed in Ge at 1.06 μm. Note that this dependence is not described by our theory, but results from the details of the damage process which lead to a modification of the initial surface roughness, and thus change the parameters s and F. Our theory can then, with these modified parameters, be used to understand the onset of further damage. In the case of Ge the surface defects apparently evolve until they conform to an $s \simeq 0.4$, $F \simeq 0.7$ description, at which stage the redistribution effect in the regions near localized defects becomes great enough to produce a large inhomogeneous energy deposition capable of altering the resolidified surface structure (cf. Fig. 12). This process tends to occur on the inner edge of the initial annulus first since it is there that the minimum amount of redistribution of energy is required to prevent the melting of portions of the surface, which would otherwise melt. Once these fringes are established near the edge, a simple feedback mechanism would allow their propagation towards the center despite the fact that the ambient intensity there is sufficient to uniformly melt the sample to a significant depth. Once some surface damage has been produced by a laser pulse the surface also contains a peak in its Fourier spectrum, $b(\vec{\kappa})$ coincident with the peak in $\eta(\vec{\kappa})$ which was initially responsible for the damage. The combined effect of $b(\vec{\kappa})$ and $\eta(\vec{\kappa})$ probably makes the surface that much more efficient at redistributing the energy from subsequent pulses. This increase in efficiency likely only occurs up to the stage where the induced damage depth becomes comparable to the wavelength, at which point it is difficult to predict what happens, since our theory is no longer valid. Experiments indicate that steady-state patterns only exist over a narrow intensity range so that it appears that once the ripples extend to a certain depth, approximately equal to the wavelength, further pulses tend to cause their deterioration.

VI. CONCLUSIONS

The process whereby very well-defined periodic damage patterns are formed on various nominally smooth solid surfaces upon their irradiation by different wavelengths of laser radiation has been studied both experimentally and theoretically. It is found that the Fourier transform of the damaged region provides information about the surface structure not previously recognized. With the use of the Fourier transforms as a basis of comparison, it is found that the damage produced in Ge, Si, Al, and brass at wavelengths of 1.06 and 0.53 μm are strikingly similar. The damage patterns develop spatially and temporally as a series of laser pulses strike the surface. This evolutionary process studied on a shot-to-shot basis indicates that the initial surface preparation is unimportant in determining the steady-state damage patterns produced as long as the surface is not rough on the scale of the wavelength of light. Based on the premise that the damage is due to periodic energy deposition in a pattern similar to that of the resulting damage, the observed diffraction patterns were compared to the inhomogeneous intensity distribution patterns calculated using the light-scattering theory described in the preceding paper of this series.[17] Very good agreement between theory and experiment is found. Not only can we explain the condition (1) for periodic damage, special cases of which have been a puzzle in the literature for the last seventeen years, but our predictions for the intensity distribution of the damage among values of $\vec{\kappa}$ that satisfy equation (1) is quite impressive; for s-polarized damaging beams the agreement is achieved without any adjustable parameters, while for p-polarized light the parameters that are required to fit most of the data are in agreement with a scenario for the temporal evolution of the damage. Most of the points that cannot be explained in terms of the theory, such as the very strong type-c fringes in Ge at 1.06 μm, are probably linked to the role of feedback and the details of the actual damage mechanism that exists for each ma-

terial. It is in the consideration of these latter two processes that we feel the further study of this phenomenon is most likely to progress. As a final note, we mention that the inhomogeneous energy deposition discussed in this work will presumably be present at fluence levels too low for permanent damage to occur. There are, therefore, important implications in this work to many aspects of the interaction of radiation with matter. This interesting general feature of the interaction of radiation with a surface, and its consequences are matters we plan to address in future work.

ACKNOWLEDGMENTS

We gratefully acknowledge research support from the Natural Sciences and Engineering Research Council of Canada including awards of a scholarship to J. F. Y. and J. S. P.

[1]B. E. Newman, Laser Focus 18 (2), 53 (1982).

[2]*Laser and Electron Beam Processing of Materials,* edited by C. W. White and P. S. Peercy (Academic, New York, 1980).

[3]C. W. White, J. Narayan, and R. T. Young, Science 204, 461 (1979).

[4]M. Birnbaum, J. Appl. Phys. 36, 3688 (1965).

[5]D. C. Emmony, R. P. Howson, and L. J. Willis, Appl. Phys. Lett. 23, 598 (1973).

[6]H. J. Leamy, G. A. Rozgonyi, T. T. Sheng, and G. K. Celler, Appl. Phys. Lett. 32, 535 (1978).

[7]G. N. Maracas, G. L. Harris, C. A. Lee, and R. A. McFarlane, Appl. Phys. Lett. 33, 453 (1978).

[8]M. Oron and G. Sorensen, Appl. Phys. Lett. 35, 782 (1979).

[9]J. F. Young, J. Sipe, M. I. Gallant, J. S. Preston, and H. M. van Driel, in *Laser and Electron Beam Interactions With Solids,* edited by B. R. Appleton and G. K. Celler (North-Holland, Amsterdam, 1982), p. 233.

[10]P. M. Fauchet and A. E. Siegman, Appl. Phys. Lett. 40, 824 (1982).

[11]T. E. Zavecz and M. A. Saifi, Appl. Phys. Lett. 26, 165 (1975).

[12]J. C. Koo and R. E. Slusher, Appl. Phys. Lett. 28, 614 (1976).

[13]N. R. Isenor, Appl. Phys. Lett. 31, 148 (1977).

[14]A. K. Jain, V. N. Kulkarni, D. K. Sood, and J. S. Uppol, J. Appl. Phys. 52, 4882 (1981).

[15]P. A. Temple and M. J. Soileau, IEEE J. Quant. Elec. QE-17, 2067 (1981).

[16]J. A. van Vechten, Solid State Commun. 39, 1285 (1981).

[17]J. Sipe, J. F. Young, J. S. Preston, and H. M. van Driel, Phys. Rev. B 27, 1141 (1983).

[18]J. F. Young, J. Sipe, J. Preston, and H. M. van Driel, Appl. Phys. Lett. 41, 261 (1982).

[19]Most values taken from *American Institute of Physics Handbook,* edited by D. E. Gray (McGraw-Hill, New York, 1972).

[20]J. M. Liu, R. Yen, H. Kurz, and N. Bloembergen, Appl. Phys. Lett. 39, 755 (1981).

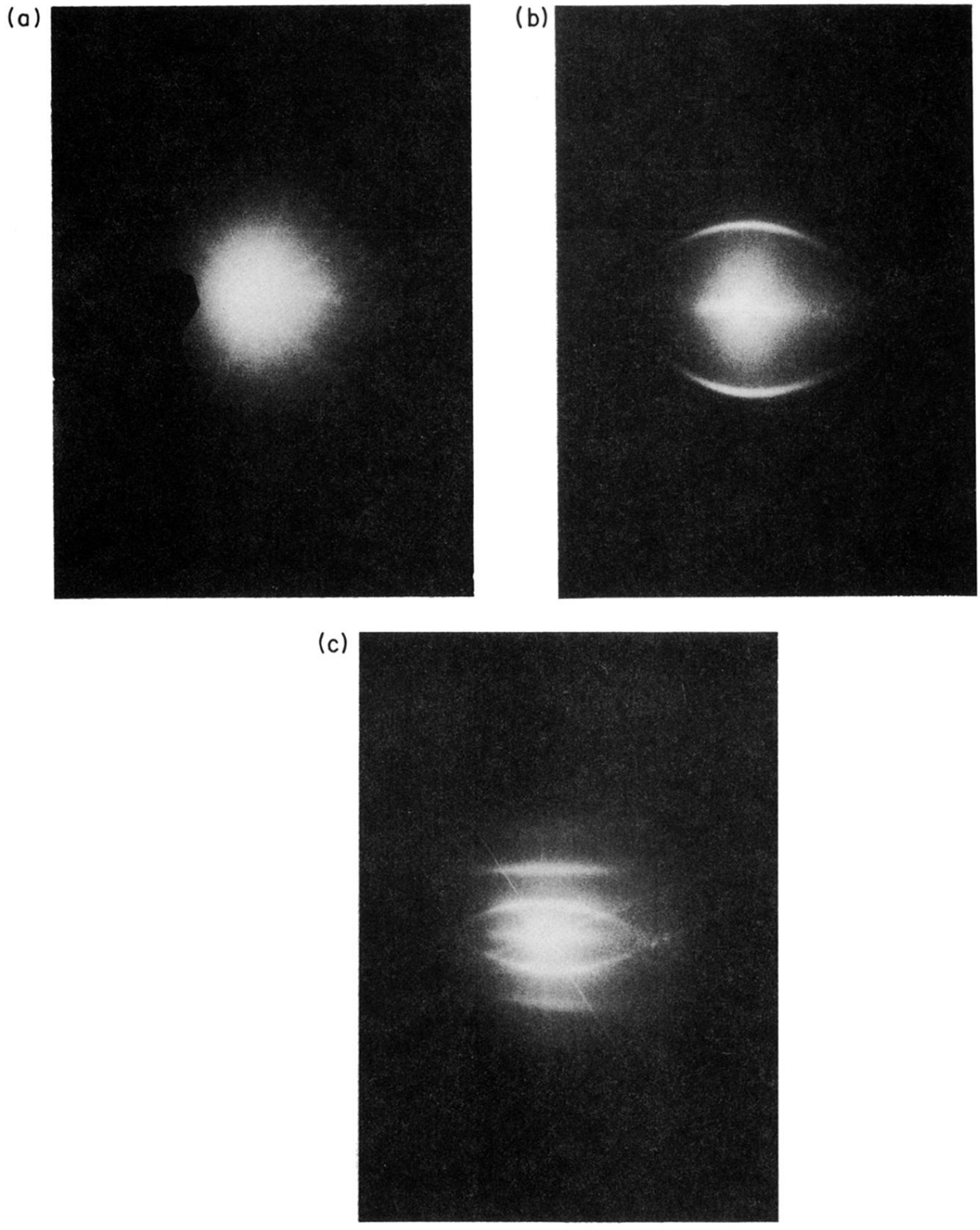

FIG. 10. Diffraction patterns produced from Al irradiated by p-polarized, 0.53-μm radiation incident at (a) 0°, (b) 30°, and (c) 60°. The shadow is that of the sample in a holder.

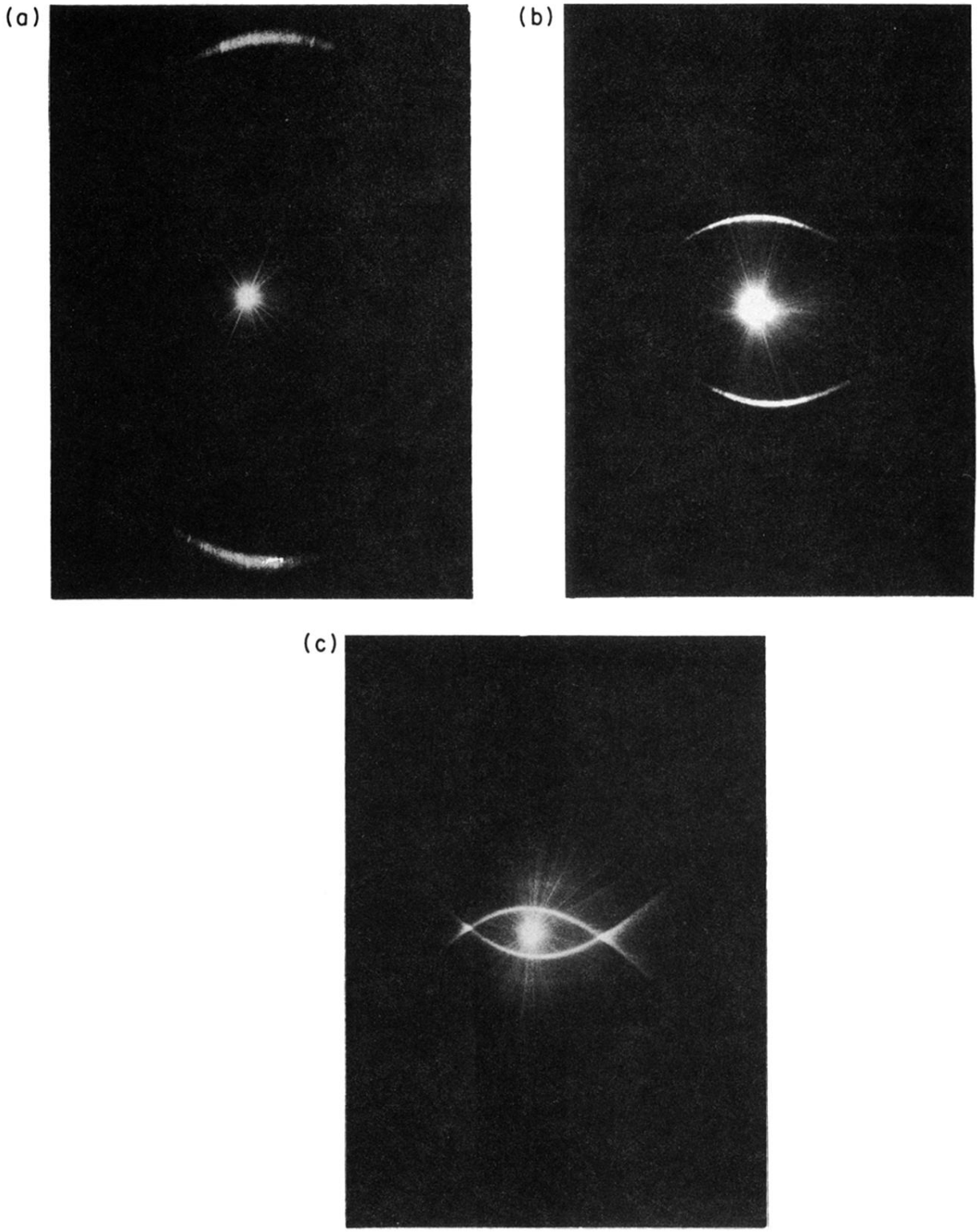

FIG. 11. Diffraction patterns produced from Ge irradiated by p-polarized, 0.53-μm radiation incident at (a) 0°, (b) 30°, and (c) 60°.

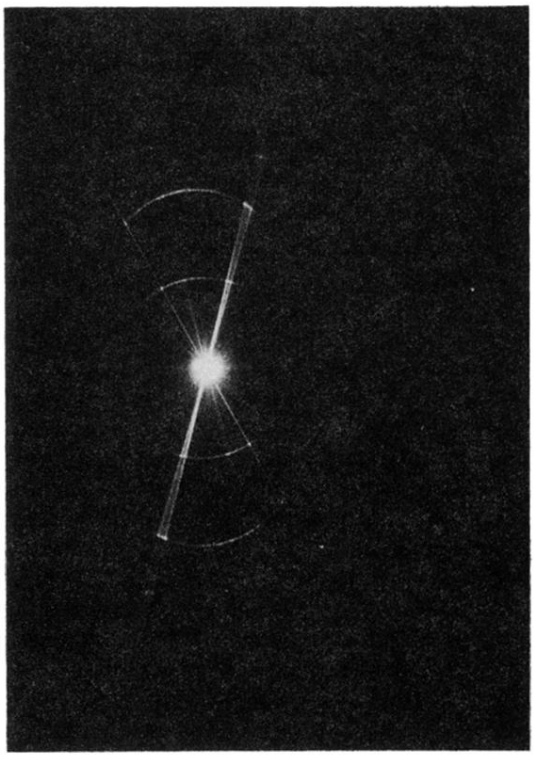

FIG. 12. Diffraction pattern produced from a Ge surface preferentially scratched in a number of discrete directions prior to irradiation by five shots of p-polarized 1.06-μm radiation incident at 15°. Note the radial lines corresponding to the diffraction from the randomly spaced, but nearly parallel scratches. Note also the bright spots at the intersections of these radial lines with the "usual" fringe diffraction pattern.

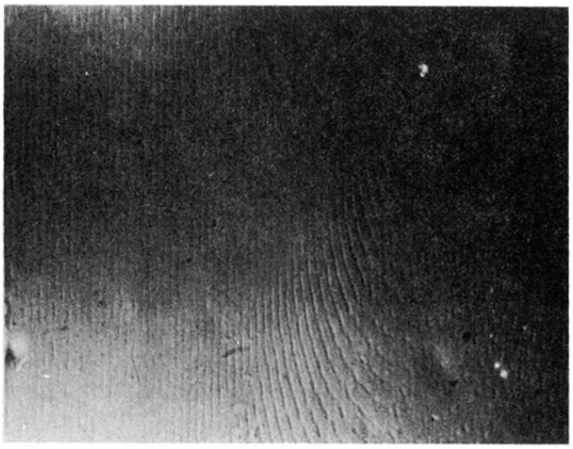

FIG. 13. Photograph of a portion of the Ge surface after being hit by 10 pulses 0f 1.06-μm, p-polarized radiation. Note how the fanlike pattern emanating from the localized defect continuously transforms into the parallel, type-c fringes which eventually dominate.

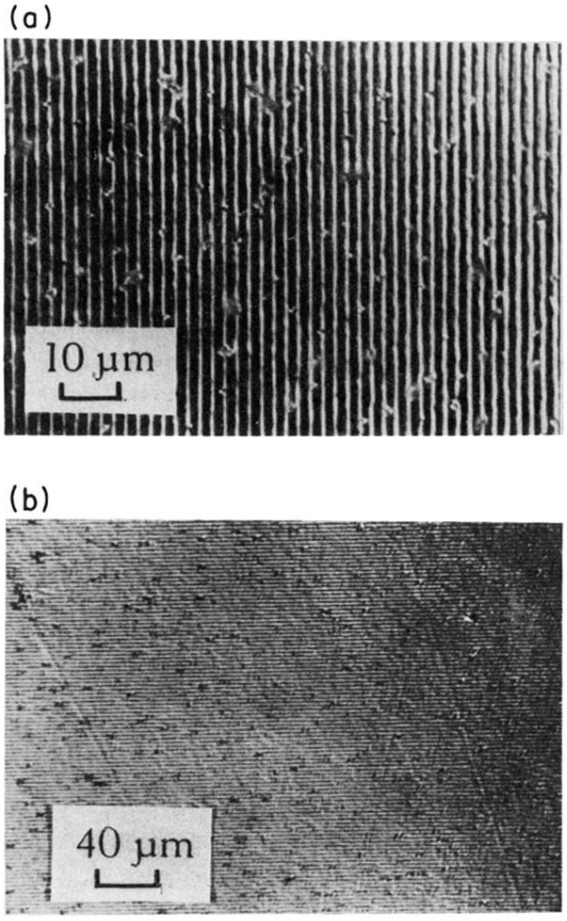

FIG. 2. Photographs of the strong type-*c* fringes produced in Ge with *p*-polarized light incident at an angle of 60°. The magnification in (a) is 4× that of (b).

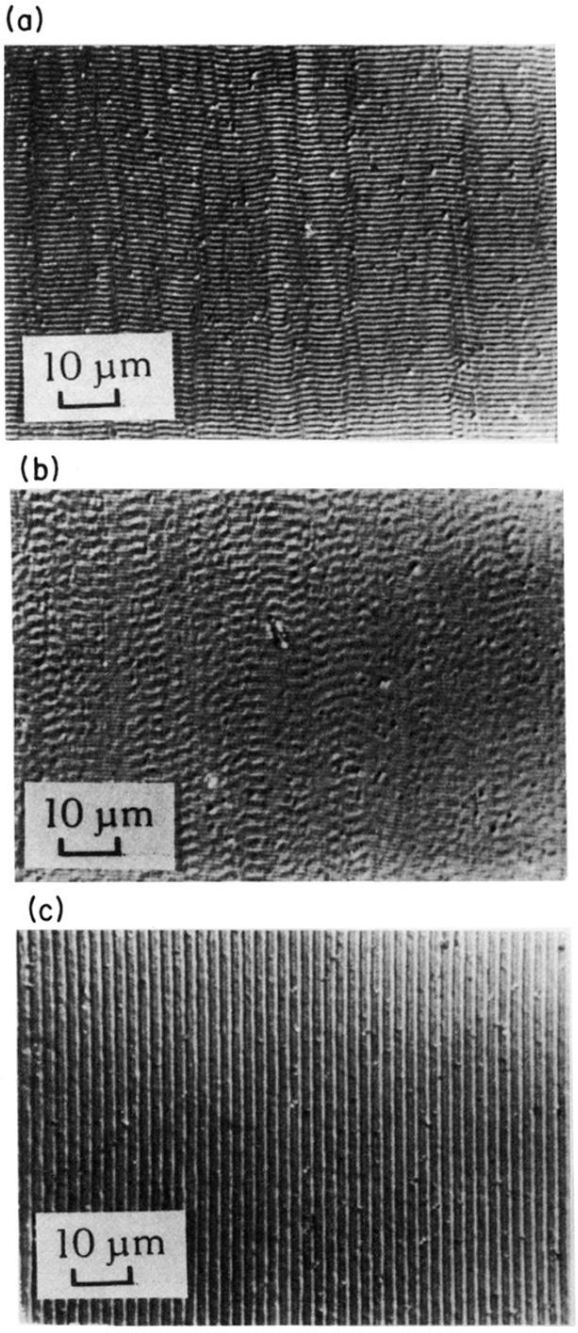

FIG. 4. Photographs of the surface structure produced on Ge with p-polarized 1.06-μm radiation incident at angles of (a) 0°, (b) 30°, and (c) 60°. Close inspection of (b) reveals both the type-s^+ and -s^- fringe patterns.

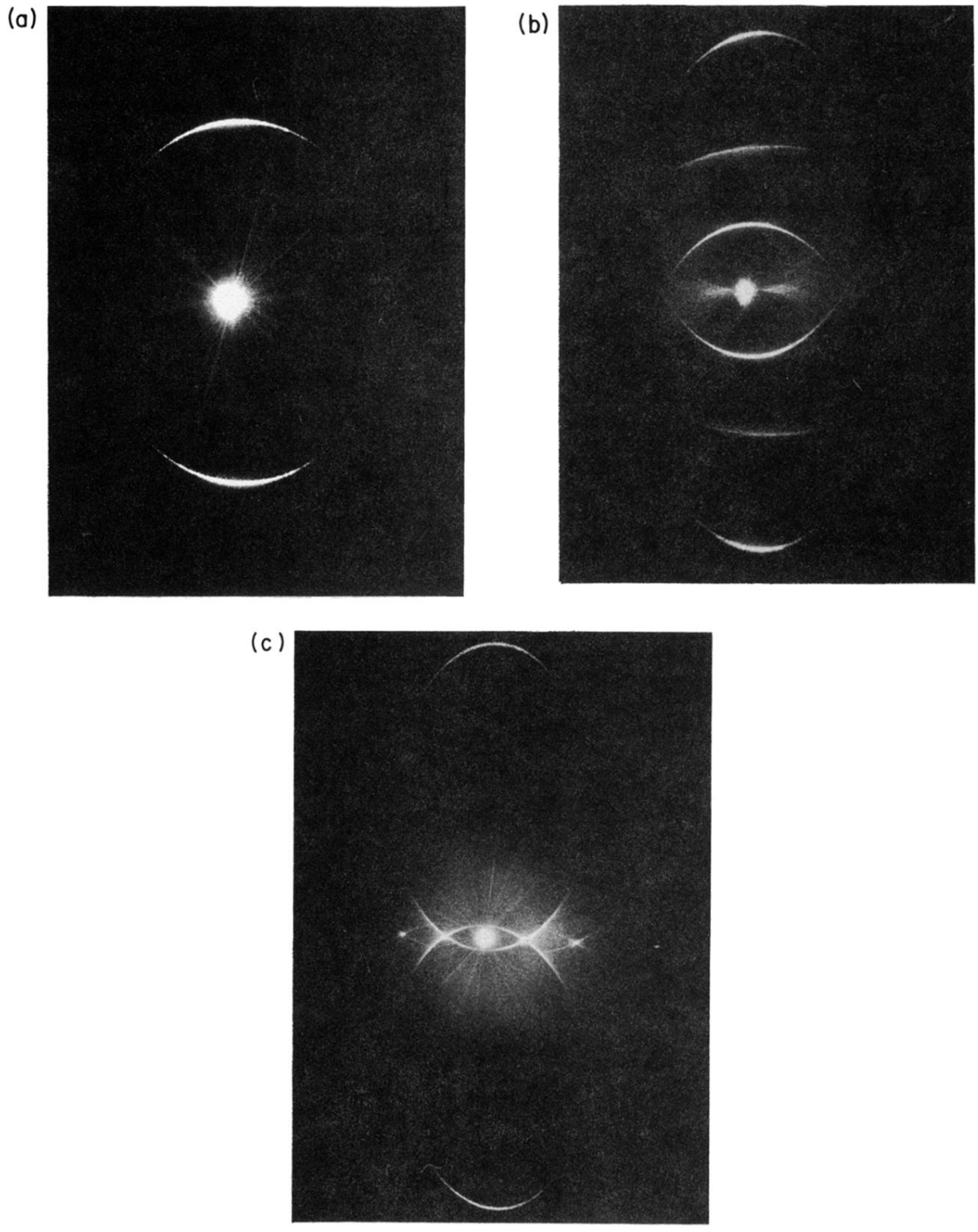

FIG. 5. Photographs of the diffraction patterns produced on the screen of Fig. 1 from the samples shown in Figs. 4(a), 4(b), and 4(c) are shown in (a), (b), and (c), respectively. Note that all photographs of the diffraction patterns were taken at an angle with respect to the screen which introduces some distortion.

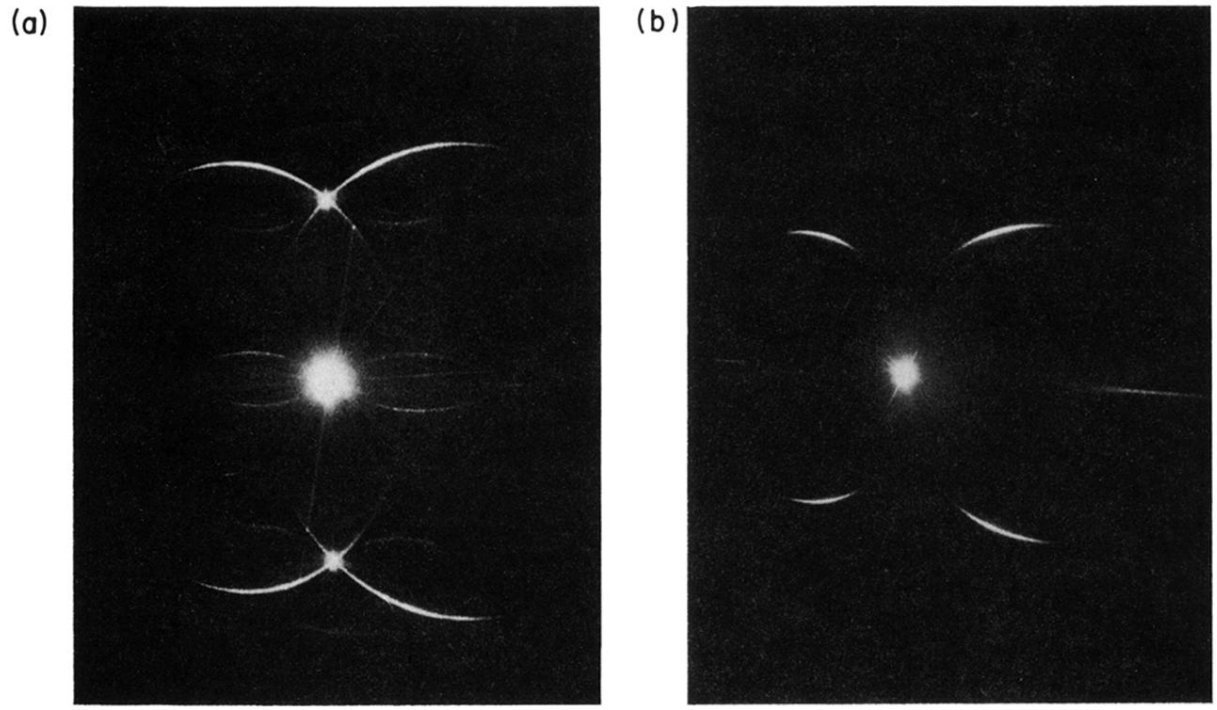

FIG. 6. Photographs of diffraction patterns produced by Ge samples which were irradiated with *s*-polarized 1.06-μm radiation incident at (a) 30° and (b) 60°.

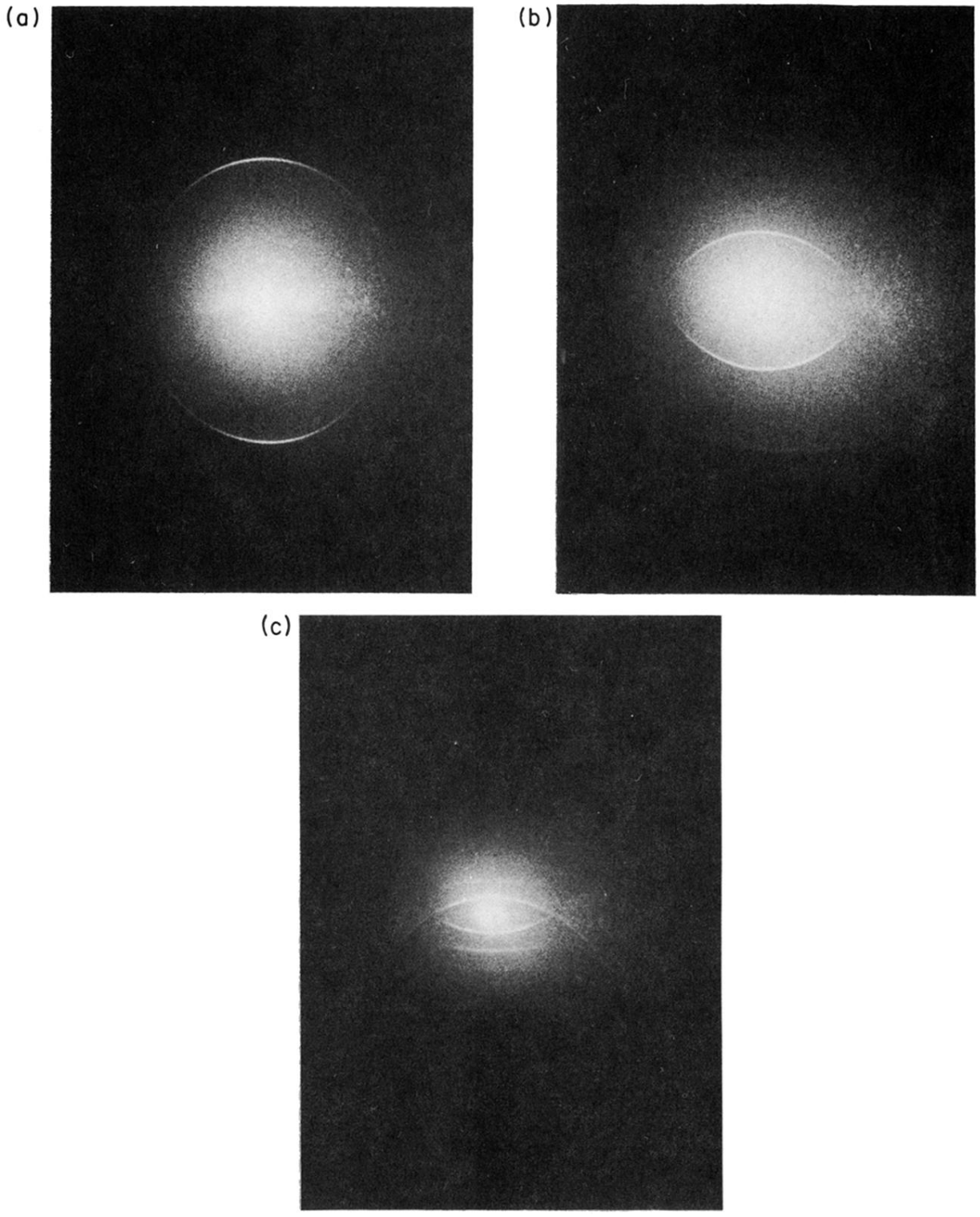

FIG. 9. Diffraction patterns produced from Al irradiated with p-polarized, 1.06-μm radiation incident at (a) 0°, (b) 30°, and (c) 60°.